

# Multi-Phase Characterization of Asphalt Concrete using X-ray Microfluorescence

Sanjeev Adhikari<sup>1</sup>, Zhanping You<sup>2+</sup>, and Karl Peterson<sup>3</sup>

**Abstract:** The objective of this study was to develop a microstructure characterization technique to capture the multi-phase nature of asphalt concrete using x-ray microfluorescence. This study examines the morphology and positions of aggregates, sand mastic and air void phases of asphalt concrete. Three different samples with targeted air void levels of 4%, 7%, and 10% were analyzed using an X-ray microscope. The cylindrical asphalt specimens were cut into slabs and then polished, and finally white zinc-oxide powder was pressed into the voids. The zinc-oxide powder helped to discern air voids from aggregate and mastic. After sample preparation, elemental maps were constructed using characteristic  $K\alpha$  x-rays from the following elements: aluminum, silicon, sulfur, chlorine, potassium, calcium, iron, zinc, and strontium. The relative intensities of pixels in the elemental maps were used to categorize pixels in each image according to sand mastic, air voids, and aggregate using multi-spectral analysis techniques. Air void contents in the three images (A, B and C) are correlated to those computed from the asphalt concrete. It was found that the air void contents in the three images (A, B) are highly correlated to those computed from the asphalt concrete. The images were utilized to calculate aggregate gradations and compared with the real gradation. It is concluded that the microstructure characterization technique to capture the multi-phase nature of asphalt concrete using x-ray microfluorescence was moderately successful.

**DOI:** 10.6135/ijprt.org.tw/2013.6(2).117

**Key words:** Air void; Aggregate; Asphalt concrete; Image processing; Microstructure; Sand mastic; X-ray microfluorescence.

## Introduction

Asphalt concrete is prepared by mixing together graded aggregate (coarse and fine aggregate) with asphalt cement content and then compacted to get a specific percentage of air void level. The basic components of asphalt concrete are divided into graded aggregate, binder and air void. Fine aggregates of the graded aggregate are embedded in the matrix of asphalt binder and referred to as sand mastic. Therefore, there are three phases of material in the asphalt concrete's microstructure: aggregate (or coarse aggregate), sand mastic and air void. The physical and mechanical properties of asphalt concrete depend upon the quantities and mechanical properties of the individual constituents. Aggregate shape, gradation and orientation also play an important role.

It is challenging to get accurate data for the morphology and positions of aggregate, sand mastic and air void phases of asphalt concrete. Images of the microstructure can be obtained from a flat-bed scanner, X-ray computed tomography (CT), or X-ray microfluorescence. Image processing techniques are then employed to acquire the aggregate, mastic and air void shape and orientation. You and Buttlar [1] and You et al. [2] captured the asphalt concrete 2D microstructure using optical grayscale scans of smoothly sawn

asphalt concrete specimens. Image analysis software was used to process and analyze the images to identify the sand mastic and aggregate skeleton of the image. An aggregate size larger than 1.18 mm was selected as the minimum aggregate size in the aggregate skeleton. Therefore, the mastic included all the aggregates finer than 1.18mm. The air void content was not measured from the scanned image, as the edges of air voids were difficult to discern on a saw-cut surface [2].

X-ray CT is a very useful technique to analyze aggregate orientation, aggregate gradation, sand mastic distribution, and air void distribution in the asphalt mixture. Detailed descriptions of x-ray CT technology are provided by various researchers such as Desrués et al. [3] and Raynaud et al. [4]. Part et al. [5] used x-ray CT to show the homogeneity and isotropy of gyratory compacted asphalt concrete specimens. X-ray CT imaging is an advanced technique acquiring successive cross sectional images from the material in a non-destructive fashion. Many researchers have used x-ray CT imaging techniques to characterize asphalt concrete in recent years [6-11]. X-ray CT images are very useful technique to model the asphalt concrete. It has been used to predict the dynamic modulus of asphalt mixture using 2D and 3D discrete element modeling (DEM) as a starting point [12-13]. The main drawback of X-ray CT is that the equipment is prohibitively expensive, and therefore difficult to adopt by every researcher.

The phases of asphalt concrete (aggregate, sand mastic, and air void) can also be easily separated using X-ray microfluorescence. The X-ray microscope utilizes an X-ray flux that is intensified and focused through a guide tube. A rhodium target provides the source of X-ray radiation. Some of the incoming  $Rh K\alpha$  X-rays interact with electrons in the sample, producing lower energy x-rays characteristic of the chemical composition of the sample. Other x-rays pass through the sample. Sutter et al. [14] used X-ray microfluorescence for

<sup>1</sup> Department of Applied Engineering and Technology, Morehead State University, 210 Lloyd Cassity, Morehead, KY 40351, USA.

<sup>2</sup> Department of Civil and Environmental Engineering, Michigan Technological University, 1400 Townsend Drive, Houghton, Michigan, 49931-1295, USA.

<sup>3</sup> Department of Civil Engineering, University of Toronto, 35 St. George Street, Toronto, Ontario, M5S1A4, Canada.

<sup>+</sup> Corresponding Author: E-mail zyou@mtu.edu

Note: Submitted July 7, 2012; Revised October 5, 2012; Accepted October 9, 2012.

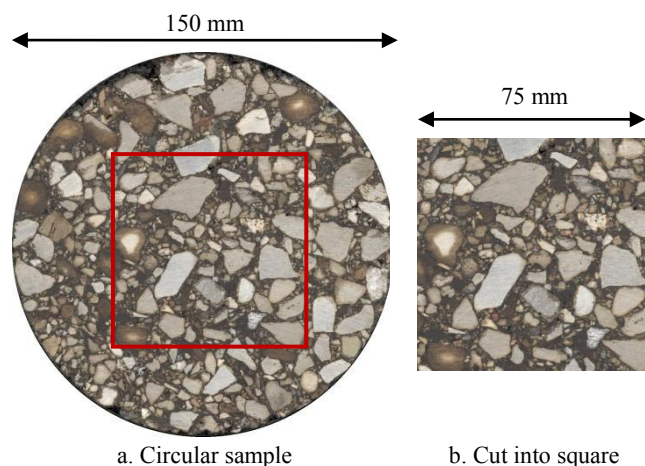


**Fig. 1.** Illustration of Compacted Cut Samples.



**Fig. 2.** X-ray Scanning Microscope.

determining chloride ion profiles of portland cement concrete. Clark et al. [15] used X-ray transmission microcopy to study high resolution images of hydrating cement pastes structures of cement concrete.

X-ray microcopy is an innovative technique to study the asphalt concrete microstructure. It is comparatively cheaper than X-ray computed tomography, but provides information from only a single cross-sectional plane. This study concentrated on the analysis of asphalt concrete using X-ray microfluorescence to obtain the positions and morphology of aggregate, sand mastic and air voids.

## Objective and Scope

The objective of this study is to develop a microstructure characterization technique to capture the multi-phase nature of asphalt concrete using X-ray microfluorescence. In this study, the air void, aggregates, and sand mastic phases of the asphalt concrete was obtained using two dimensional images. Three different samples with targeted air void levels of 4%, 7%, and 10% were analyzed using an X-ray microscope.

## Preparation of Asphalt Concrete

The asphalt mixture studied in this research was of gradation of a 12.5mm nominal maximum aggregate size (NMAS) used in Michigan. Aggregate was limestone. Asphalt concrete is prepared

by mixing together graded aggregate (coarse and fine aggregate) with asphalt cement content and then compacted to get a specific percentage of air void level. The mixture used PG 58-28 binder with an asphalt content of 5.60%. The mixing and compaction temperatures were fixed according to the viscosities of temperature at 154°C and 130°C, respectively, which was described in the Superpave mix design (SP2) [16].

The asphalt mixture was compacted using a gyratory compactor to a target air void level of 4%, 7%, and 10%. The compaction of asphalt mixture was designed with the estimated traffic level of more than 10 million estimated single axle loads (ESALs). The gyratory compaction number of a target air void of 4%, 7% and 10% were designed with 53, 28, and 15 gyrations, respectively. The calculated air void level was determined as 3.69%, 8.31% and 9.35% using the theoretical maximum specific gravity,  $G_{mm}$  and bulk specific gravity  $G_{mb}$ . The dimensions of the gyratory compacted cylindrical specimens were a height of 160 mm and a diameter of 150 mm. The cylindrical specimens were then cut into prisms with dimensions of 75 mm by 75 mm by 25 mm. The analyzed surface was at middle level of specimen. The 3 specimens were compared at the same level. An illustration of compacted and cut samples is shown in Fig. 1.

One face of each prism was polished by using a water-cooled rotating lap with diamond embedded platens, followed by silicon carbide adhesive backed paper. The grit sizes of the diamond embedded platens were 60, 100, 200, 300, 400 and 500. The final polish was performed on the rotating lap with a silicon carbide adhesive backed paper with a grit size of 600. The polishing steps provided a smooth cross-section through the asphalt concrete, allowing for better determination of the edges of air voids and aggregates. After polishing, ZnO powder was pressed into the air voids of the polished surface. Since ZnO is white in color, it exhibits high contrast with the darker appearance aggregate and black image of mastic. More importantly, the Zn content of the powder is easily detected by x-ray microfluorescence techniques. Prismatic stickers were placed at the corner on each polished surface. The stickers were used to align images collected with the X-ray microscope, and images collected with an ordinary desktop flatbed scanner.

## X-ray Microscope

A Horiba/Oxford XGT 2000W X-ray Analytical Microscope was used, as shown in Fig. 2. The X-ray analytical microscope employs X-ray fluorescence for qualitative and quantitative chemical analysis. The X-ray microscope uses a high intensity X-ray beam with a diameter ranging from 10  $\mu\text{m}$  to 300  $\mu\text{m}$ .

X-ray fluorescence images are obtained by moving the sample in a raster pattern beneath the fixed incoming x-ray flux. The X-ray guide tube utilizes a rhodium target that produces characteristic Rh  $K\alpha$  and  $L\alpha$  radiation at 20.217 and 2.696 keV respectively. The X-rays interact with the target material in a variety of ways, with each spatial point providing specific information of material microstructure.

## Scanning and Image Processing Technique

Images from the three asphalt concrete specimens (labeled A, B and C) were collected using a typical office desktop flatbed scanner, and

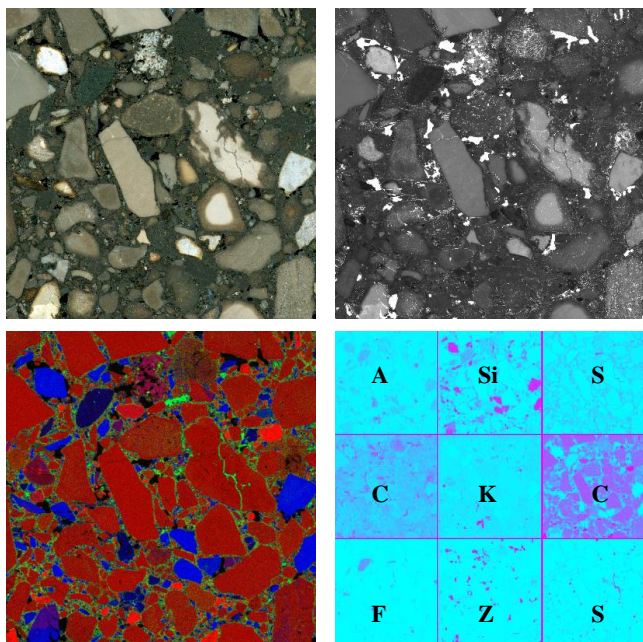


**Fig. 3.** 60 x 60 mm Image A. Clockwise from the Upper Left: Scanned Color Image of Slab as Polished, Scanned Black and White Image of Slab After Pressing ZnO Powder in the Voids, Summary of Elemental Maps, False Color RGB Image where The Ca Map is Assigned to the Red Channel, The S Map is Assigned to The Green Channel, and the Si Map is Assigned to the Blue Channel.

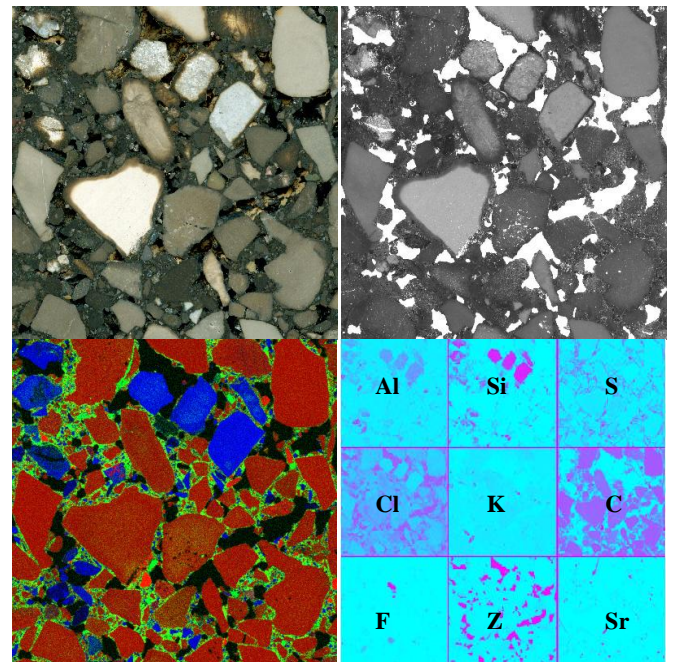


**Fig. 5.** 60 x 60 mm Image C. Clockwise from the Upper Left: Scanned Color Image of Slab as Polished, Scanned Black and White Image of Slab after Pressing ZnO Powder in The Voids, Summary of Elemental Maps, False Color RGB Image where The Ca Map is Assigned to the Red Channel, the S Map is Assigned to The Green Channel, and the Si Map is Assigned to the Blue Channel.

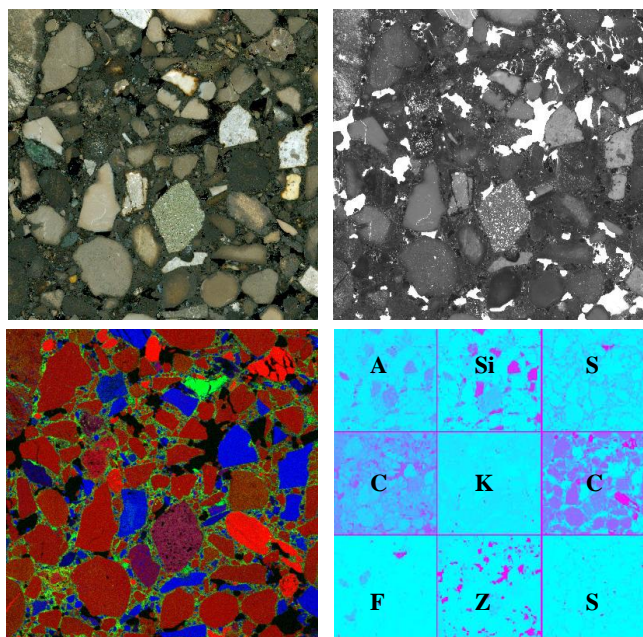


**Fig. 4.** 60 x 60 mm Image B. Clockwise from the Upper Left: Scanned Color Image of Slab as Polished, Scanned Black and White Image of Slab after Pressing ZnO Powder in the Voids, Summary of Elemental Maps, False Color RGB Image where The Ca Map is Assigned to the Red Channel, the S Map is Assigned to The Green Channel, and The Si Map is Assigned to the Blue Channel.

the X-ray microscope. An accelerating voltage of 50kV and a current of 1.0 mA were used to generate characteristic x-rays from the rhodium target. The x-rays were collimated to a 300 micrometer

spot size on the polished surface. A motorized stage was used to step the polished surfaces beneath the x-ray source, covering an area of 60 x 60 mm with a step size of 150 micrometers and a dwell time of 137 microseconds per pixel. The flatbed scanner images were collected at a resolution of 24 dpm.

An energy dispersive spectrometer (EDS) was used to collect X-rays generated due to interactions between the polished surface and the incoming X-ray source. Elemental maps were constructed using characteristic  $K\alpha$  X-rays from the following elements: aluminum, silicon, sulfur, chlorine, potassium, calcium, iron, zinc, and strontium. Characteristic  $K\alpha$  X-rays generated from elements of atomic number lower than aluminum are for the most part absorbed by air prior to reaching the EDS, and were omitted from the elemental mapping procedure. Rhodium  $L\alpha$  x-rays occur at energy very close to chlorine  $K\alpha$  x-rays, so the majority of the signal observed in the elemental map for chlorine was actually due to Rayleigh scattering of the incoming rhodium  $L\alpha$  X-rays. The top halves of Figs. 3 through 5 show optical scanned images of the slabs as polished and after the introduction of ZnO powder. The bottom halves of Figs. 3 through 5 include summaries of the elemental maps, and false-color images constructed using the elemental maps for calcium, sulfur, and silicon.

The relative intensities of pixels in the elemental maps and scanner images were used to categorize pixels in each image according to mastic, voids, and aggregate using multi-spectral image processing software. To categorize each image, small regions representative of the mastic, voids, and aggregate were selected by the operator. The statistics of the intensity levels of the populations of pixels defined by the operator were subsequently used to

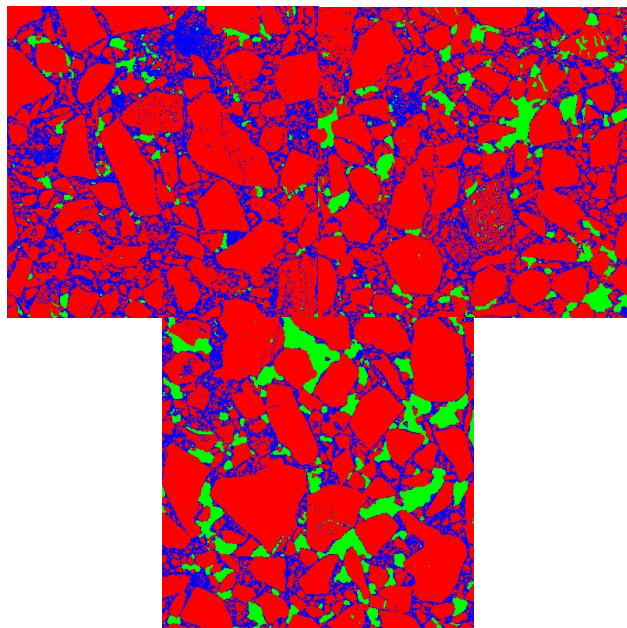


**Fig. 6.** 60 x 60 mm Classified Images from Image A, (top left) Image B, (Top Right) and Image C, (Bottom) Asphalt Concrete Samples where Mastic Appears Blue, Voids Appear Green, and Aggregates Appear Red.

**Table 1.** Volume Percentage of Air Void, Aggregate and Mastic Calculated from the Images.

Image	Air void, %	Mastic, %	Aggregate, %
A	2.78	25.70	71.52
B	8.18	20.71	71.11
C	12.79	18.29	68.93

**Table 2.** Volume Percentage of Air Void, Aggregate and Mastic Calculated from The Asphalt Concrete and Aggregate Blends.

Mix	Air void, %	Mastic, %	Aggregate, %
A	3.69	30.21	66.10
B	8.31	25.59	66.10
C	9.35	24.55	66.10

automatically classify each pixel in the entire image as either mastic, void, or aggregate using a minimum distance to means approach, [17, 18]. Fig. 6 shows the classified images of aggregate, mastic and void derived from the element maps.

It should be noted that the majority of the aggregate present in polished slabs originated from a dolomite quarry with abundant celestite (strontium sulfate) deposits. A large coarse aggregate particle of arsenopyrite (FeAsS) was observed in the sample prepared from asphalt concrete sample C (note the strong sulfur and iron signals for the particle in the upper-right quadrant of the elemental map summary in Fig. 5). A large coarse aggregate particle of blast furnace slag was observed in the sample prepared from the asphalt concrete sample A (note the irregularly shaped porous particle near the top-middle of the optical scanned images in Fig. 3).

### Microstructure Analysis

The volume percentages of air void, aggregate, and sand mastic

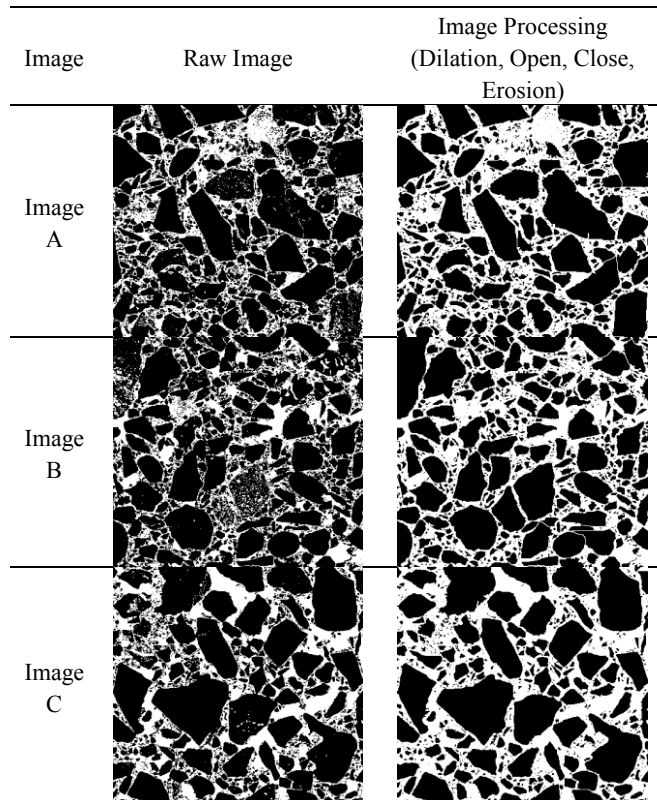


**Fig. 7.** Aggregate Structure of Raw Image and after Image Processing.

domains calculated from the images collected from the three different asphalt specimens are listed in Table 1. The calculated air void content of image A image was lower than the value calculated using the theoretical maximum specific gravity. The air void contents of images B and image C were higher than the values calculated using the theoretical maximum specific gravities. Table 1 shows that the sand mastic and aggregate percentages decrease when the air void level is increased. Therefore, it can be concluded that the air voids were developed within the matrix of mastic. Table 2 shows volume percentage of air void, aggregate and mastic calculated from the asphalt concrete and aggregate blends. The air void level was determined using the theoretical maximum specific gravity,  $G_{mm}$  and bulk specific gravity  $G_{mb}$ . The volume of aggregate and mastic was calculated from the specific gravity and weight of the mastic and aggregate. The specific gravity of the mastic is 2.09 and asphalt mixture is 2.358. We try to correlate air void contents in the three images to those computed from the asphalt concrete. It was found that the air void contents in the three images (A, B) are highly correlated to those computed from the asphalt concrete. The mastic volumes in the images are also highly correlated to the lab data. Air void calculated from image C slightly over-predicted the real air void. Clearly, the 2D cross-sectional area represented is not an accurate represent of the true dimensions in 3D, rather only an approximation.

### Aggregate Gradation Analysis

Aggregate gradation and aggregate orientation of images A, B and C were analyzed by image processing techniques. Morphological

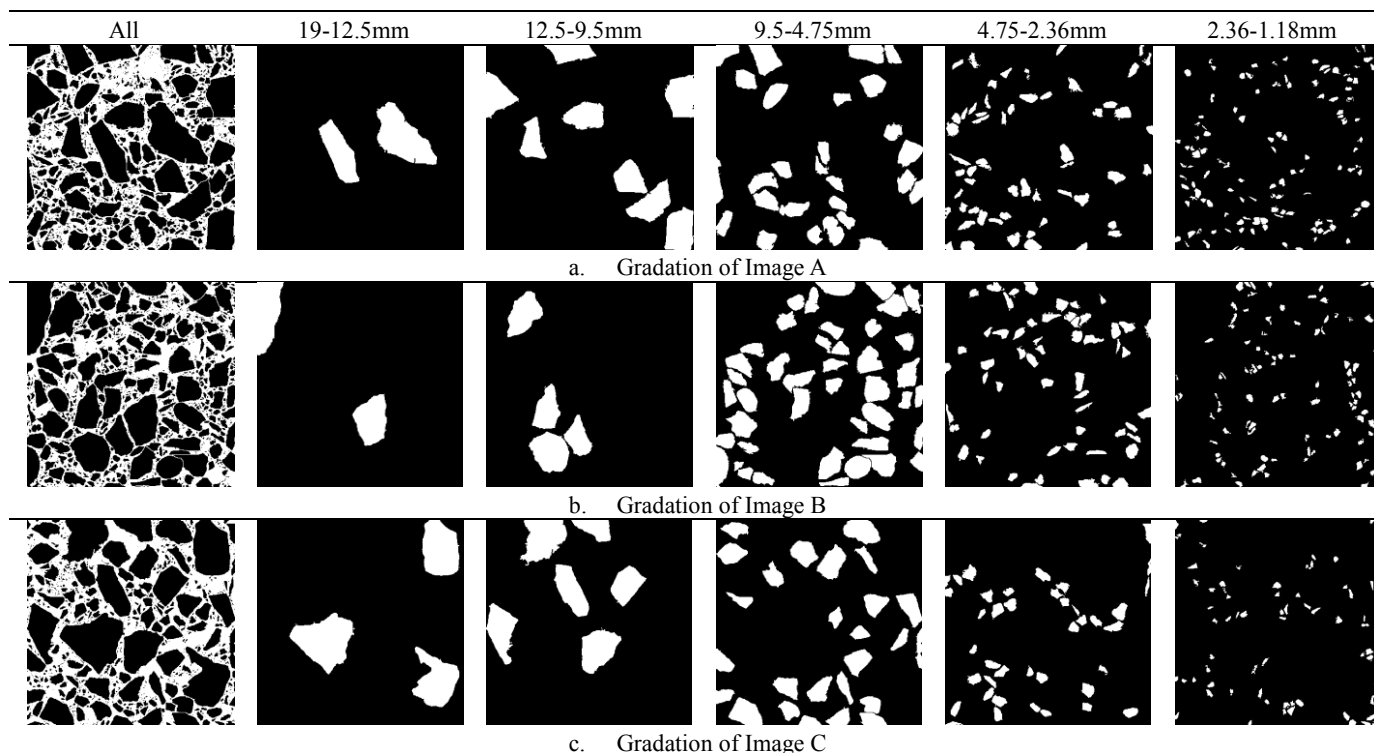


Fig. 8. Gradation of Aggregates Captured from Image Processing.

Table 3a. Comparison of Real Gradation with Gradation Calculated from 2D Images.

Sieve Size, mm	Retaining of Lab Mix, %	Retaining on Image A, %	Retaining on Image B, %	Retaining on Image C, %
19	0	0	0	0
12.5	14.7	11.05	8.84	19.01
9.5	14.3	22.32	12.00	20.75
4.75	27.2	26.19	42.17	29.36
2.36	17.9	13.25	13.98	11.19
1.18	8.4	9.69	9.01	6.28

Table 3b. Difference between Calculated of Real Gradation with Calculated 2D Images

Lab Mixture and Image A	Lab Mixture and Image B	Lab Mixture and Image C
0	0	0
3.65	5.86	-4.31
-8.02	2.3	-6.45
1.01	-14.97	-2.16
4.65	3.92	6.71

filters such as erosion, dilation, and combinations thereof, (opening and closing) were used to clarify and isolate aggregate as shown in Fig. 7 [18].

The digitally filtered images were utilized to calculate a gradation for the aggregate and compare with the real gradation of aggregate. The gradation of aggregate was determined by percentage retained in different sieve sizes according to volume. For the gradation analysis, aggregate size can be defined by the polygon average diameter, minimum diameter, maximum diameter, maximum length,

minimum length, major axis, minor axis, minimum feret (shortest caliper length) maximum feret (longest caliper length) etc. In this study, the average of the polygon diameter was chosen as a threshold to determine which aggregates would be “retained” on a given sieve. Naturally, such an approach does not reflect the true gradation, since it is based on a two dimensional slice through a three dimensional system; i.e. the diameter of any given particle is in all cases either equal to or less than the true diameter of the particle. In spite of this obvious shortcoming, the different sizes of aggregate captured from image processing routine are shown in Fig. 8. The separate aggregate according to sieve sizes was studied for image A, B and C. The retaining aggregate size 12.5, 9.5, 4.75, 2.36 and 1.18mm of the three different images are compared in Table 3. It was difficult to capture aggregate less than 1.18 mm. When we compare retaining on Sieve size 4.75, Image A and Image C has very close with real gradation. Image B over-predicted with real gradation. Clearly, the 2D cross-sectional area represented is not an accurate represent of the true dimensions in 3D, rather only an approximation.

### Summary and Conclusion

The objective of this study was to develop a microstructure characterization technique to capture the multi-phase nature of asphalt concrete using x-ray Microfluorescence. Through this study, the air void, aggregates, and mastic phases of the asphalt concrete can be obtained using two dimensional images. Therefore the technique will not require the expensive x-ray computed tomography equipment. In this study, x-ray Microfluorescence was used to capture three phases of asphalt concrete. A qualitative look at the classified images suggests that the method presented for

classifying digital images according to sand mastic, voids, and aggregate was moderately successful. The air void contents of the three samples studied in this paper are highly correlated to the actual air void level of the asphalt concrete. The mastic volume percentages are also very close to the actual measurements. This indicates that the 2D images prepared with the proposed technique can be useful to obtain asphalt concrete air void, aggregate, and mastic volumetric data.

It is also indicated that the application of this method to asphalt concrete produced with blends of various types of aggregates is perhaps inappropriate; the method could be more successfully implemented on asphalt concrete produced with a single source of aggregate. If the source of aggregate was uniformly light-colored in appearance, such as a white marble or quartzite, it is likely that optical scanned images, both before and after the white powder treatment, would be sufficient to classify the image, eliminating the need for X-ray elemental mapping. Although not performed here, a quantitative assessment of the accuracy of the classified images could be conducted using a standard method where the identities of points on the polished slab are identified under a stereo-microscope by a human operator as sand mastic, void, or aggregate, and compared to the same pixel locations in the classified image.

The scanned three images were utilized to calculate gradation of aggregate and compared with the real gradation. When comparing the predicted and real gradation, the gradation calculated from Image A compared well with the real gradation. The gradation calculated from image B slightly under-predicted the real gradation and the gradation calculated from image C slightly over-predicted the real gradation. Clearly, the 2D cross-sectional area represented by an aggregate particle is not an accurate represent of the true dimensions in 3D, rather only an approximation.

## Acknowledgements

This material is based in part upon work supported by the National Science Foundation under Grant CMMI 0701264 to Michigan Technological University. Any opinions, findings, and conclusions or recommendations expressed in this material are those of the author's and do not necessarily reflect the views of the National Science Foundation.

## References

1. You, Z. and Buttlar, W.G. (204). Discrete Element Modeling to Predict the Modulus of Asphalt Concrete Mixtures, *Journal of Materials in Civil Engineering*, 16(2), pp.140-146.
2. You, Z., Adhikari, S., and Dai, Q. (2008). Three-Dimensional Discrete Element Models for Asphalt Mixtures, *Journal of Engineering Mechanics*, 134(12), pp. 1053-1063.
3. Desrues, J., Chambon, R., Mokmi, M., and Mazerolle, F. (1996). Void ratio evolution inside shear bands in triaxial sand specimens studies by computed tomography, *Geotechnique*, 46(3), pp. 529-546.
4. Raynaud, S., Fabre, D., and Mazerolle, F. (1989). Analysis of the internal structure of rocks and characterization of mechanical deformation by a non-destructive method: x-ray tomodensitometry, *Tectonophysics*, 159, pp. 149-159.
5. Partl, M.N., Flisch, A., and Jönsson, M. (2003). Gyrotory Compaction Analysis with Computer Tomography, *International Journal of Road Materials and Pavement Design*, 4(4), pp. 401-422.
6. Shashidhar, N. (1999). X-ray tomography of asphalt concrete, *Transportation Research Record*, No. 1681, pp. 186-192.
7. Braz, D., Lopes, R.T., and da Motta, L.M.G. (2000). Computed tomography: an evaluation of the effect of adding polymer SBS to asphaltic mixtures used in paving, *Applied Radiation and Isotopes*, 53(4), pp. 725-729.
8. Shi, B., Murakami, Y., Wu, Z., Chen, J., and Inyang, H. (1999). Monitoring of internal failure evolution in soils using computerization X-ray tomography, *Engineering Geology*, 54(3), pp. 321-328.
9. Masad, E., Jandhyala, V.K., Dasgupta, N., Somadevan, N. and Shashidhar, N. (2002). Characterization of Air Void Distribution in Asphalt Mixes Using X-Ray Computed Tomography, *Journal of Materials in Civil Engineering*, 14(2), pp. 122-129.
10. Tian, L., Liu, Y., and Wang, B. (2007). 3D DEM model and digital restructure technique for asphalt mixture simulation, *Journal of Changan University, Natural Science Edition*, 27(4), pp. 23-26.
11. Wang, L., Frost, J.D., and Shashidhar, N. (2001). Microstructure Study of Westrack Mixes from X-ray Tomography Images, *Transportation Research Record*, No. 1767, pp. 85-94.
12. Adhikari, S. and You, Z. (2008). 3D Microstructural Models for Asphalt Mixtures Using X-Ray Computed Tomography Images, *International Journal of Pavement Research and Technology*, 1(3), pp. 94-99.
13. You, Z., Adhikari, S., and Kutay, M.E. (2008). Dynamic Modulus Simulation of the Asphalt Concrete Using the X-Ray Computed Tomography Images, *Materials and Structures*, 42(5), pp. 617-630.
14. Sutter, L.L., Dam, T.J.V., Peterosn, K.R., and Ganguly, A. (2003). The X-ray microscope: A new tool for determining chloride ion diffusion in hardened concrete, in *Advanced in Cement Concrete, Engineering Conference International*. Copper Mountain, Colorado, USA.
15. Clark, S.M., Morrison, G.R., and Shi, W.D. (1999). The use of scanning transmission X-ray microscopy for the real-time study of cement hydration, *Cement and Concrete Research*, 29, pp. 1099-1102.
16. Asphalt Institute (1996). Superpave Performance Graded Asphalt Mix Specification and Testing, *Journal of Materials in Civil Engineering*.
17. Jensen, J.R. (1996). *Introductory Digital Image Processing: A Remote Sensing Perspective*, Prentice Hall, Upper Saddle River, New Jersey, USA.
18. Adhikari, S. and You, Z. (2010). The Sensitivity of Aggregate Size within Sand Mastic to Model the Microstructure of Asphalt Mixture. *Journal of Materials in Civil Engineering*, 23(5), pp.580-586.